Proceedings of the
Annual Stability Conference
Structural Stability Research Council
Atlanta, Georgia, April 21-24, 2020

The interaction of section and member slenderness on the behavior of high strength composite filled tube (CFT) members

Abdullah M. Alghossoon[1], Amit H. Varma[2]

Abstract
This paper's primary focus is on the interaction of member and section slenderness on the behavior and design of high-strength composite filled tube (CFT) members, including columns, beams, and beam-columns. The goal is to include the member slenderness and high material strength into the design equations. Besides, developing simplified stress blocks and establishing the column design curve and axial force-bending moment (P-M) interaction curve in line with the current design code methodology. Design variables were investigated by conducting a parametric study covering 15000 cases, including: (1) member (global) slenderness; (2) section slenderness; (3) section's aspect ratio; (4) material strength; (5) level of axial loading. The beam-column model is a 2D inelastic fiber model implemented using OpenSees software. Fibers of the cross-section utilized verified effective stress-strain curves that take into account the steel local buckling and concrete confinement in the high strength CFT members. The results from these evaluations are presented, along with fundamental insights into behavior. This paper discusses the potential simplification of these findings into design equations that can be used in everyday practice.

1. Introduction

The use of concrete-filled tube (CFT) columns as part of the lateral force-resisting system or the gravity system of high-rise buildings is of interest due to their potential stiffness, strength, and ductility in terms of deformation and strain capacity. The steel tube or box section can provide stability during construction activities and serve as stay-in-place (permanent) formwork during concrete placement. The structural-effectiveness of these filled composite columns can be improved by using higher-strength materials since the elastic stiffness of concrete increases with strength. The economic efficiency of filled composite columns can be improved by using thinner but higher-strength steel tubes. Overall, the structural and economic efficiency can be harnessed by using higher strength filled composite (CFT) columns with non-compact or slender cross-sections. However, there is limited research on the behavior, analysis, and design of such members, particularly the interaction of local and global slenderness on the behavior and strength of high strength CFT members.

[1] Ph.D. student, Purdue University, <aalghoss@purdue.edu>
[2] Professor, Purdue University, <ahvarma@purdue.edu>

There has been significant interest in the behavior of high strength CFT columns in the recent past. Researchers (including the authors) have proposed phenomenological (effective) stress-strain curves for the steel and concrete materials that can implicitly model the effects of yielding, local buckling, biaxial stresses, concrete confinement, and crushing. These effective stress-strain curves have been used to investigate and evaluate the behavior of high strength CFT members. However, the investigations were limited to short members with little to no global slenderness effects.

The AISC 360-16 code addresses the behavior of the conventional strength CFT columns extensively in the case of low-section slenderness (compact section). Numerical and experimental investigations have been done by Lai and Varma (2016), to investigate the behavior and design of slender and noncompact CFT columns using conventional material strength. More recently, (Lai and Varma 2018) proposed an effective stress-strain curve for high strength stub CFT columns, which is the one adopted in the study's fiber model. Mursi and Uy (2004) investigated the influence of using a high strength steel box filled with conventional concrete strength on the performance of 4 stub CFT columns under axial loading and four slender CFT columns under eccentric axial loading. Liu et al. (2007) investigated the use of high concrete strength in the rectangular CFT column (68-84 Mpa), they concluded the high conservative results in estimating the strength of these CFT columns using the AISC design equations. The influence of the member slenderness was addressed by Patel et al. (2012) where they presented a numerical model for simulating the behavior of high-strength thin-walled CFT slender beam-columns considering the effects of local buckling, column slenderness ratio, depth-to-thickness ratio, loading eccentricity ratio, concrete compressive strengths, and steel yield strengths.

The current AISC does not endorse the use of high-strength materials nor the influence of member-slenderness in the design of CFT columns because of the lack of adequate research and comprehensive design equations. Consequently, there is a need to fill the gap that is present in the area of high strength slender CFT columns research. The authors have conducted a parametric study on a high-strength slender composite CFT member considering: (1) the global member slenderness (length-to-depth ratio, *L/D*); (2) steel-section slenderness (λ); (3) concrete strength (f_c'); (4) steel yielding (f_y); (5) section's aspect ratio (depth-to-width ratio); (6) Level of axial loading.

2. Numerical Modeling

Fiber Model in OpenSees

Parametric studies require flexibility in modeling and the capability of automated change in the study variables during analysis. OpenSees is an open-source software framework that allows users to create finite element applications and to solve difficult nonlinear problems for static and dynamic loads, McKenna et al. (2000) Besides, it provides users with various combinations of elements, material models, and analysis algorithm formulations. Considering these features, OpenSees was adopted to perform a 2D inelastic fiber analysis on the distributed plasticity model shown in Fig. 1. In fiber modeling, the structural system is divided at the cross-section and element levels; the sub-elements are connected at the boundaries through the fibers of the cross-section. These elements were assigned as a displacement-based element in order to investigate the post-peak behavior and to reduce the convergence problems during the analysis.

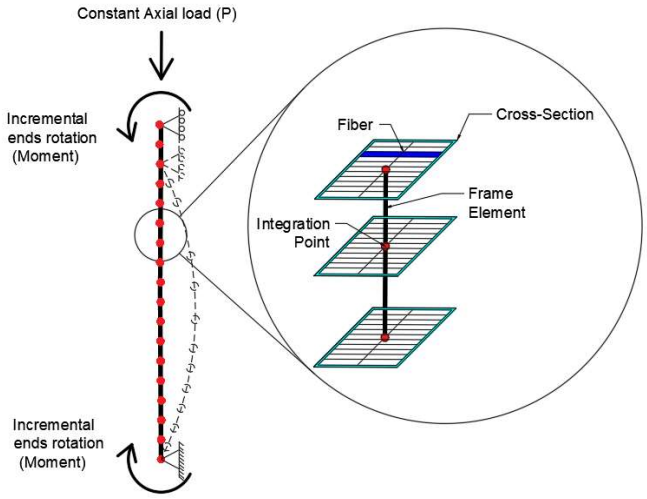

Figure 1. Fiber element modeling

This type of modeling has the advantage of distributing plasticity (yielding) over the element length and capturing the axial load-moment interaction behavior accurately. On the other hand, the accuracy of the overall behavior depends on the ability of the selected uniaxial constitutive model in capturing the deterioration phenomena such as local buckling. The effective stress-strain curves proposed by Lai and Varma (2018) for non-compact and slender high strength CFT members were selected as a constitutive material model in the model's cross-section fibers. Those curves involve a lot of experimental and numerical research that takes into consideration the local steel buckling and the concrete confinement for a wide range of parameters.

Material Stress-Strain Curve

The normalized stress-strain curves for high strength steel and high strength concrete of the rectangular CFT columns is shown in Fig. 2 and Fig. 3. Those curves were established based on a parametric study that includes three yield stresses of steel (F_y = 317, 525, and 827 Mpa), three concrete strengths ($f_c{}'$ = 21, 70, and 110 Mpa), and five slenderness ratios (*b/t = 20, 40, 60, 80, and 100*).

The steel stress-strain curve was calibrated using the Hysteretic material model available in OpenSees material library. This model possesses the required characteristics to account for the reduction in the yield strength at compression (F_{cr}) and the strength deterioration due to local buckling, as shown in Fig. 2, (a). The confined concrete stress-strain curve was calibrated using Concrete02 material model in OpenSees. The ascending branch of this model in compression is similar to that of Tao et al. (2013) models for confined concrete. Although the steel confinement does not enhance the ultimate concrete strength nor the yield plateau, it improves the concrete ductility and maintains a residual strength from the crushed concrete, as shown in Fig. 3(a). Simplified bilinear curves were assumed for fibers in tension for both steel and concrete material models. Fig. 4 demonstrates the flexibility of the OpenSees material models in simulating the effective stress-strain.

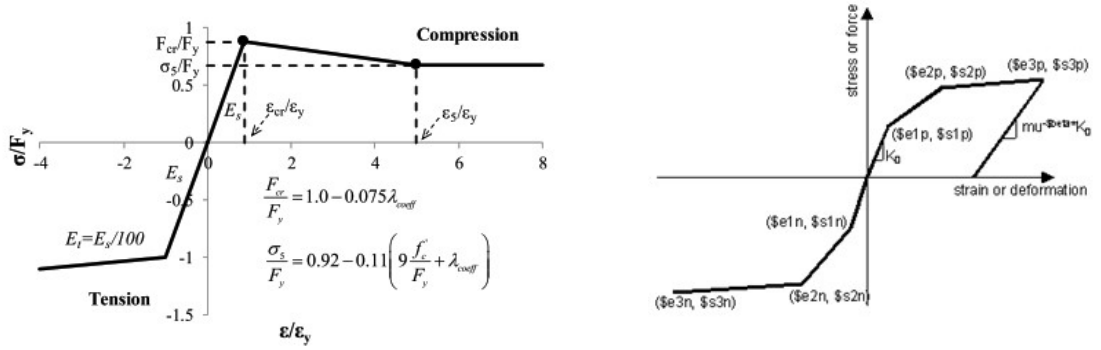

(a) (b)

Figure 2. (a) Idealized effective stress-strain relationship for high-strength steel tube in rectangular CFT columns, (b) Stress-strain curve of hysteretic material in OpenSees. (Lai and Varma (2018), OpenSeesWiki)

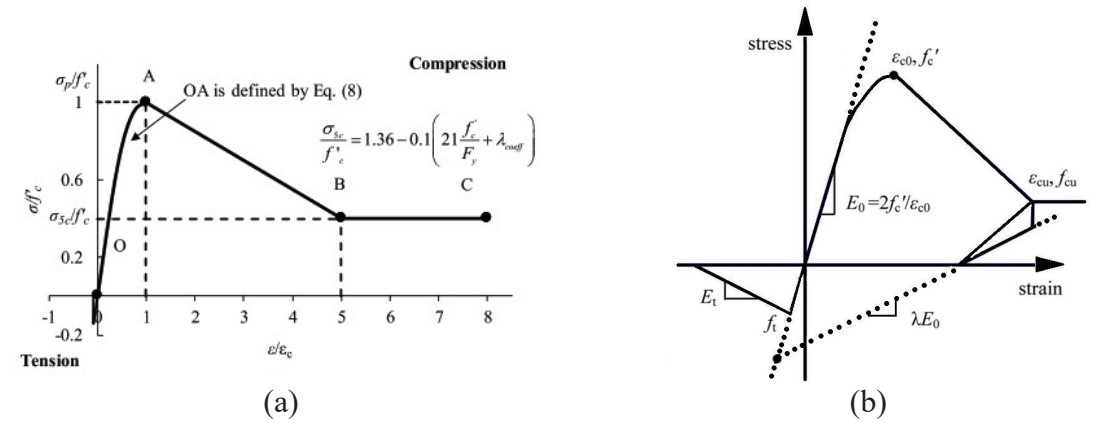

(a) (b)

Figure 3: (a) Idealized effective stress-strain relationship for high-strength concrete core in rectangular CFT columns, (b) Stress-strain curve of Concrete02 material in OpenSees. (Lai and Varma (2018), OpenSeesWiki)

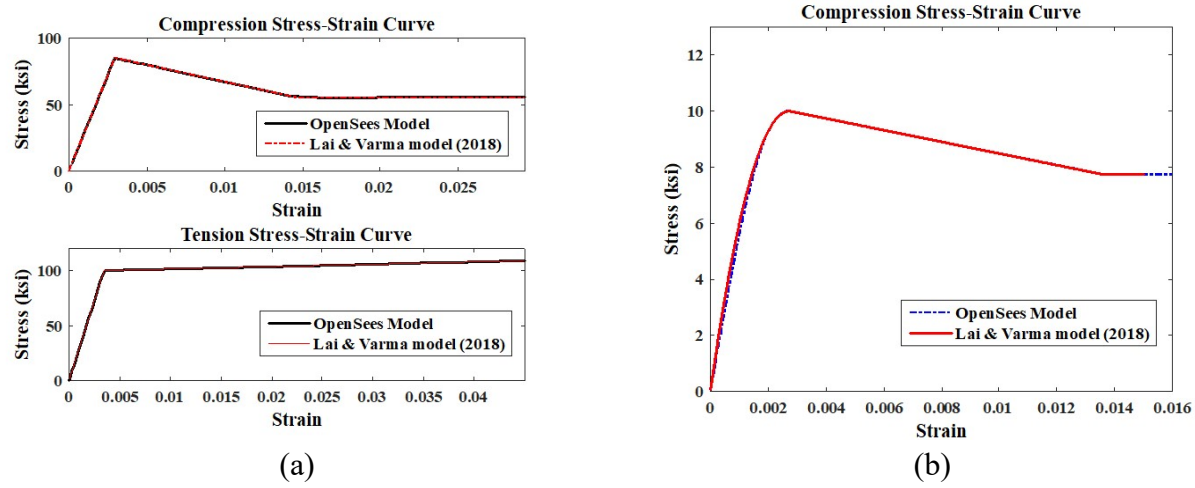

(a) (b)

Figure 4: (a) Comparison between the effective stress-strain models of high strength CFT columns and OpenSees material models, (a) Steel material model, (b) Concrete material model

Model verification

Previous experimental studies in Table 1 were compiled for modeling verification in terms of stiffness, ultimate strength, and post-peak behavior. These studies cover a wide range of parameters to generalize the validation of the study's numerical model such as member-slenderness ratio (*L/D*), section- slenderness ratio (λ), steel strength (F_y), and concrete strength (f_c'). The results of the test comparison are summarized in Fig. 5.

Table 1: Test specimens on short CFT columns with high section slenderness (λ)

Reference	Specimen	Size (mm)	F_y (Mpa)	E (GPa)	f'_c (Mpa)	b/t	P_{ult_test} (kN)	P_{ult_OS} (kN)	Ratio
Liang & Uy (1998)	NS1	186×180	300	200	32	60	1555	1555	1.0
	NS7	246×246	300	200	38	80	3095	2962	1.08
	NS13	306×300	300	200	38	100	4003	4164.0	1.04
	NS14	306×300	300	200	38	100	4003	4164.0	1.23
	NS15	306×300	300	200	38	100	4003	4164.0	1.09
	NS16	306×300	300	200	38	100	4003	4164.0	1.06
Kang et al (2001)	KOM2001	300x300	317.9	200	24.8	91.7	2749.9	2900	1.05
	KOM2001	250x250	317.9	200	24.8	91.7	2123	2222.6	1.05
	Avg								1.07

Table 2: Test specimens on short CFT columns using high material strength

Reference	Specimen	Size (mm) B=H	L (mm)	F_y Mpa	E_c GPa	f'_c Mpa	b/t	P_{ult_test} kN	M_{ult_test} kN.m	Ratio M_{ult}/M_{OS}
Varma (2002)	BC-32-46-20	305	1500	259	49.64	110	33.5	2520	606	0.93
	BC-32-46-40	305	1500	259	49.64	110	33.5	5035	543	0.99
	BC-32-80-20	305	1500	560	49.64	110	32.3	3050	933	0.9
	BC-32-80-40	305	1500	560	49.64	110	32.3	6100	806	0.95
	BC-48-46-20	305	1500	471	49.64	110	50.6	2360	597	0.98
	BC-48-46-22	305	1500	471	49.64	110	50.6	2520	629	0.94
	BC-48-80-20	305	1500	660	49.64	110	48	2740	700	1.05
	BC-48-80-40	305	1500	660	49.64	110	48	5480	574	1.12
		Avg								0.98

Table 3: Test specimens on slender CFT columns under eccentric/concentric loading conditions

Reference	Specimen	B x D x t (mm)	L (mm)	ex (mm)	ey (mm)	f'_c (Mpa)	F_y (Mpa)	P_{ult_test}	$P_{ult\text{-}OS}$	Ratio
Bridge (1976)	SCH-2	204×203.3×10	3050	0	0	31.1	290.0	2869	2848	1.0
Shakir-Khalil and Zeghiche (1989)	R5	120×80×5	2940	40	0	36.6	343.3	206	214.7	1.04
	R1	80x120x5	3210	0	0	37.4	386.3	600	601	1.0
Chung et al	C24-0	125x125x3.2	3050	0	0	94.1	450.0	1079	1155	0.94
	C30-0	125x125x3.2	3750	0	0	94.1	450.0	747	865	0.86
Matsui. et al (1995)	S1	149x149x4.27	2700	0	0	31.9	445	1355	1300	1.04
	S3	149.8×149.8×4.27	2700	0	75	31.9	445.0	552	536	0.97
	S5	149x149x4.27	3600	0	0	31.9	445	1143	1105	1.03
	S9	149x149x4.27	3600	0	0	31.9	445	909	893	1.01
	Avg									0.99

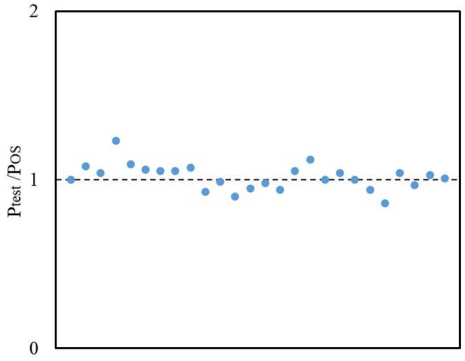

Figure 5: Comparison between OpenSees ultimate strength and Tables 1, 2,3 tests results

Fig. 6 shows the model's force-displacement curves in the same plots used by other researchers to verify their numerical models, such as Hadi. et al. (2012) and Lai and Varma (2018). The concordance between the OpenSees model and the experimental results is evident even for the long column specimens such as SCH-2, R5, and S3, where significant flexural stresses are present due to the application of eccentric axial load. Generally, the behavior of these specimens under the combined stresses was simulated satisfactorily for all specimens, even in the high inelastic deformations.

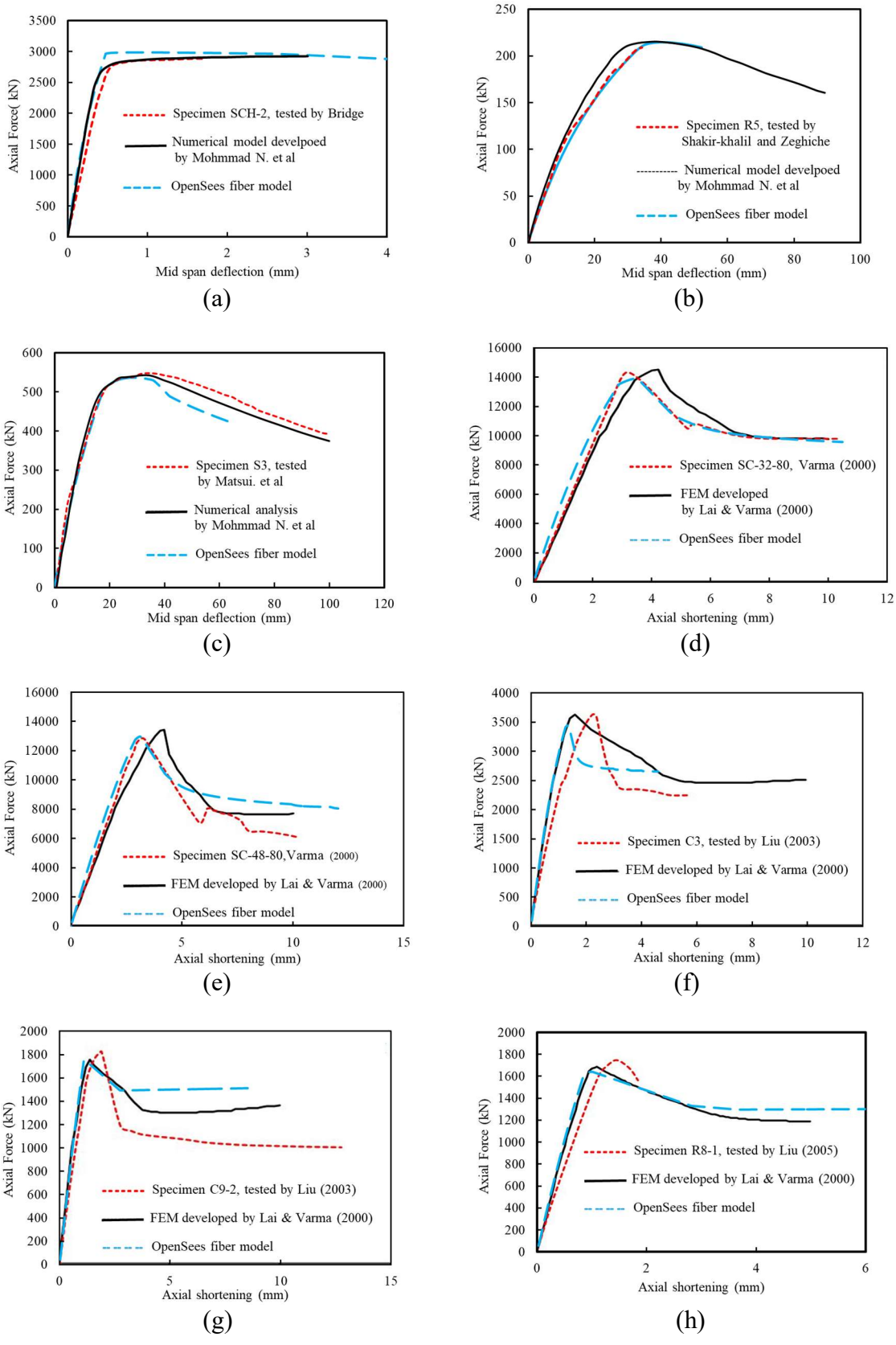

Figure 6: Comparison between OpenSees model the results of previous tests

Parametric Study

The range of parameters included in this study is shown in the parametric matrix in Table 4 below. The influence of all possible configurations of the material and the geometric properties was investigated and analyzed in the presence of different levels of axial loading. Parallel computing techniques were utilized to analyze around 15000 cases, and the output files were read and processed using (MATLAB 2018b).

Table 4: Parametric study matrix

Depth to width ratio D/B	Fy (ksi)	fc' (ksi)	Section Slenderness ratio (λ)	Member slenderness (L/D)	Level of Axial Loading
1	100	15	2	5	0%
				10	5%
1.5		12	3	15	10%
	80		4	20	.
2		10	5	30	.
				40	90%
					100%

3. Results and discussion

Maximum compressive and flexural strength

The maximum compressive and flexural strength recorded from the inelastic fiber analysis was compared with the results from the AISC 360-16 (2016) equations for conventional material strength in section I2-1b, I-2b, as shown in Fig. 7. The flexural strength at yield (M_y) was calculated based on the stress blocks proposed by Lai et al. (2014) for compact, non-compact, and the slender section, as shown in Fig. 8. It can be shown that the results are comparable in the case of low-sections slenderness but diverge significantly as the section slenderness increases. In line with the current design code methodology, the study proposes simplified stress blocks to calculate the nominal compressive and flexural strength of the high strength CFT section, as shown in Fig. 9. The proposed stress blocks are based on a plastic stress distribution over the composite cross-section with the concrete compressive stress limited to f_c'. This demonstrates the insignificant increase in strength due to the confimnment provided by the steel section. The overall section strength is governed by the critical buckling strength of the steel section (F_{cr}), which has a theoretical upper limit of F_y and varies linearly with the section slenderness (λ), as shown in Fig. 10 The continuity of the critical buckling strength function eliminates the need for the current section classification (compact, non-compact, and slender) and provides a straightforward equation to represent all the ranges of section slenderness. The study proposes Eq. 1 to Eq. 5 to calculate the nominal compressive and flexural strength of the high strength CFT section. The accuracy of the proposed equation is compared with the benchmarked OpenSees model as shown in Fig. 11.

$$F_{cr} = F_y\left(1 - 0.75\lambda\right) \qquad (1)$$

$$\lambda = \frac{b/t}{\sqrt{\frac{E}{F_y}}} \qquad (2)$$

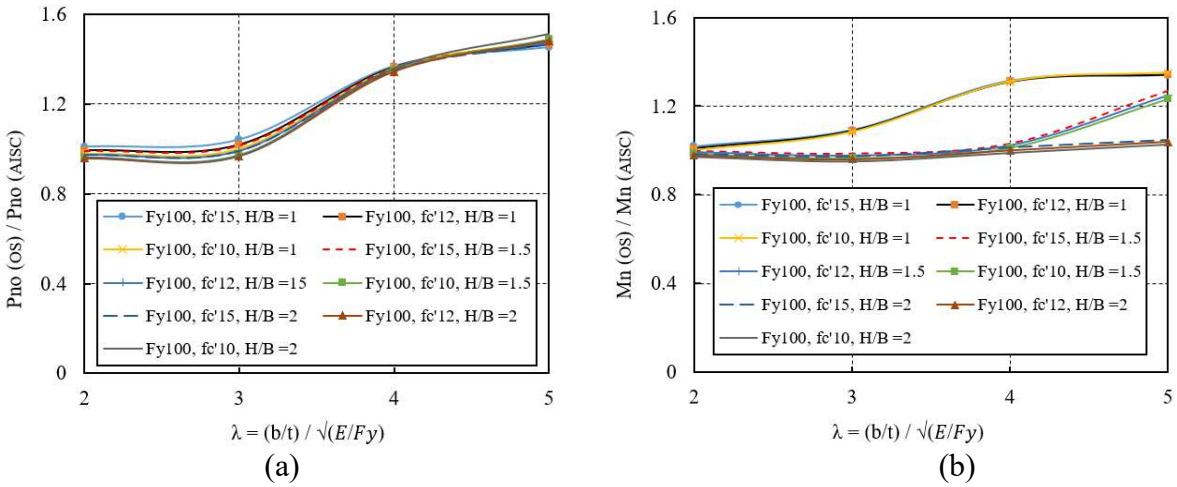

Figure 7: (a) Normalized compressive strength ($Pno_{OpenSees}/Pno_{AISC}$) vs section slenderness, (b) Normalized flexural strength ($Mno_{OpenSees}/ Mno_{AISC}$) vs section slenderness

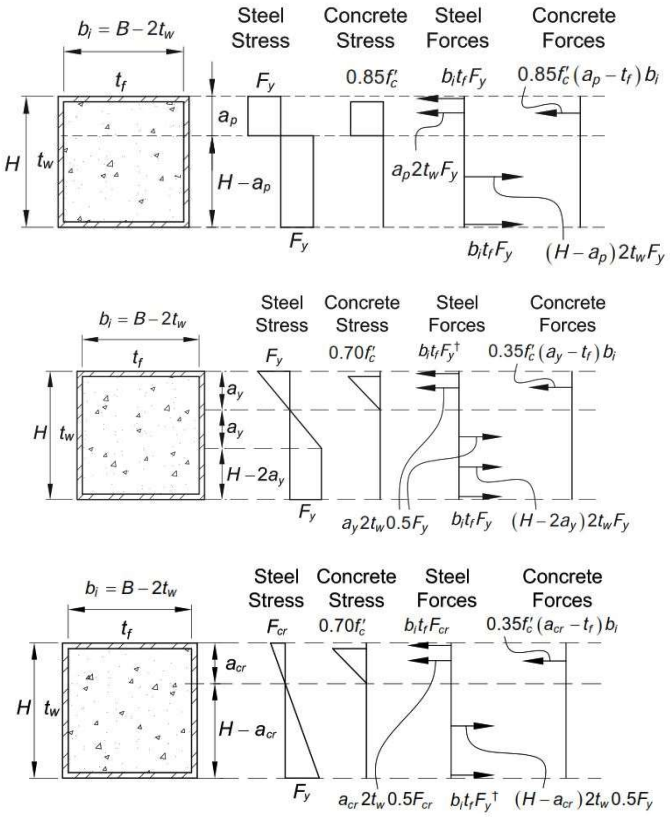

Figure 8: Stress blocks in the AISC360-16 commentary for calculating M_y for conventional strength concrete-filled rectangular box section (Lai et al., 2014)

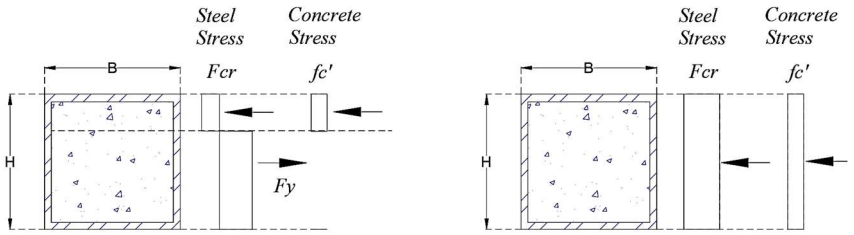

(a) (b)

Figure 9: Proposed stress blocks (a) Nominal flexural strength, (b) Nominal compressive strength

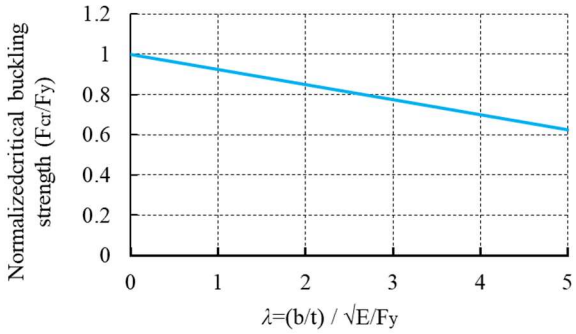

Figure 10: Critical buckling stress (F_{cr})

$$P_{no} = F_{cr}A_s + f_c'A_c \tag{3}$$

$$M_{no} = F_{cr}bt_f(a - \frac{t_f}{2}) + F_y bt_f(H - a - \frac{t_f}{2}) + F_{cr}t_w a^2 + F_y t_w(H-a)^2 + f_c'b\frac{(a-t_f)^2}{2} \tag{4}$$

$$a = \frac{2F_{cr}H t_w + f_c'bt_f}{4F_{cr}t_w + f_c'b} \tag{5}$$

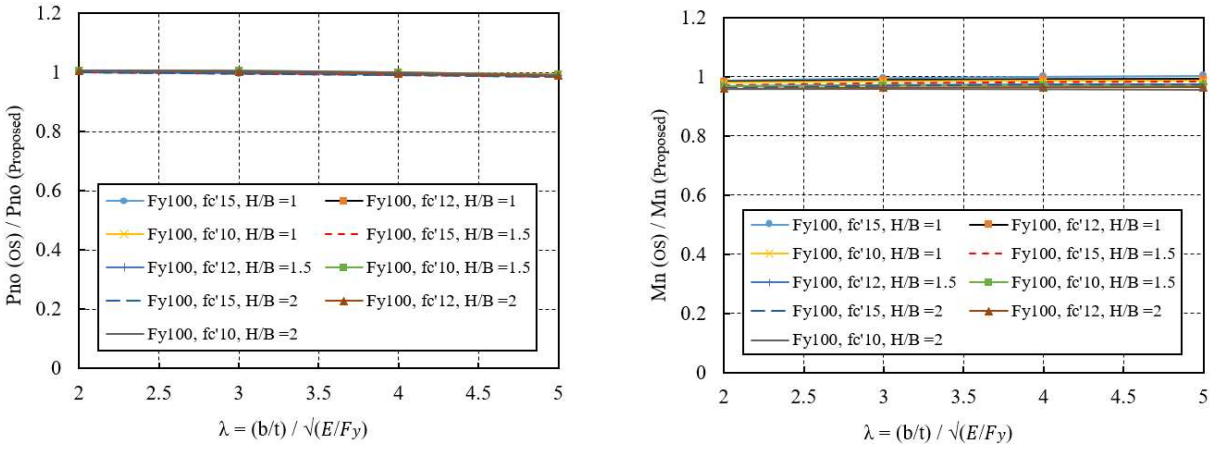

(a) (b)

Figure 11: (a) Normalized compressive strength ($Pno_{OpenSees}/Pno_{proposed}$) vs Section slenderness, (b) Normalized flexural strength ($Mno_{OpenSees}/Mno_{proposed}$) vs Section slenderness

Column design curve

The design of axially loaded members (P_n) requires investigating the compressive strength on the section-level (P_{no}) and its stability on the member-level. As the member slenderness increases, the contribution of the member's buckling strength (P_e, as a measure of its stability) increases and dominates the design strength beyond a certain point. Member slenderness ratio is a measure of the member's tendency to buckle, which can be defined in terms of the member's geometry ratio ($\frac{L}{D}$) or the member strength ratio ($\frac{P_{no}}{P_e}$). Fig. 12 demonstrates the relationship between the reduction of the member's maximum compressive strength (section strength) and the member slenderness ratio for different values of section slenderness.

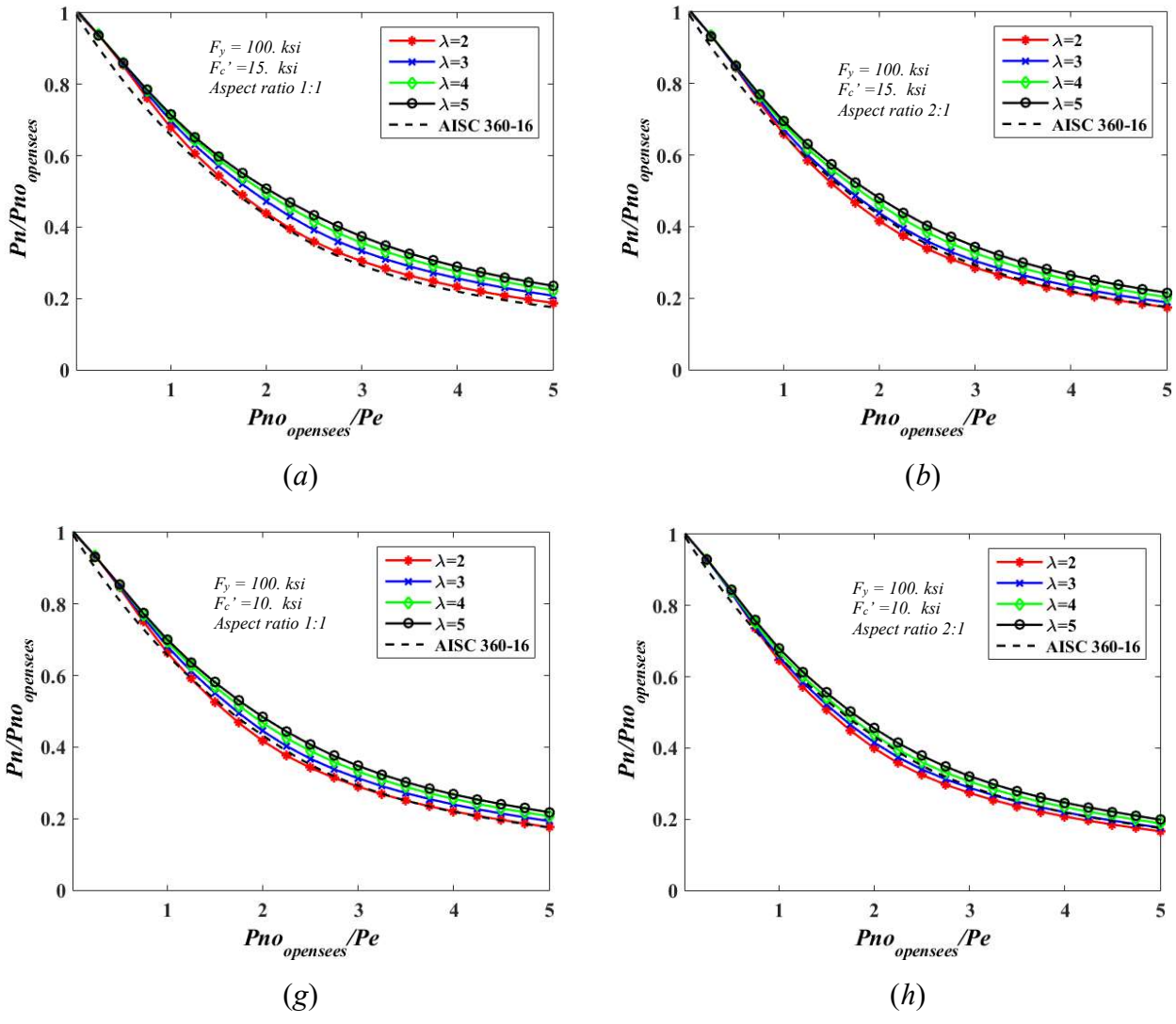

Figure 12: Normalized member compressive strength ($\frac{P_n}{P_{no}}$) vs. Section slenderness ($\frac{P_{no}}{P_e}$)

The AISC column design curve as described in Eq. 6 and Eq. 7 lines up reasonably with the study's curves in the case of low-section slenderness (compact section). The up-shifting in the higher section slenderness is attributed to the underestimation of the concrete contribution in the effective stiffness of the composite section (C_3in the AISC). The determination of the concrete contribution is quite complex and depends on the location of the neutral axis at that moment. The authors attempted to propose a more accurate equation for estimating the concrete contribution in the effective stiffness of high-strength CFT columns. The proposal in Eq. 9 includes the concrete strength along with the section slenderness term used in the AISC equation. In the light of the small variation in the values of C_3, an average value of 0.85 was found to be sufficient for estimating the axial strength, which is comparable with a previous study by Mark D. Denviat et al. (2014) who has alternatively proposed a constant value of 0.9 for CFT columns. High values for the concrete contribution can be used confidently in the case of high net compressive stresses (column region) but might lead to an unconservative error where the beam-behavior dominates.

$$\text{(a) For } \frac{P_{no}}{P_e} \le 2.25$$

$$P_n = P_{no}(0.658^{(P_{no}/P_e)}) \tag{6}$$

$$\text{(b) For } \frac{P_{no}}{P_e} > 2.25$$

$$P_n = 0.877P_e \tag{7}$$

$$C_3 = 0.45 + 3\left(\frac{A_s + A_{sr}}{A_g}\right) \le 0.9 \tag{8}$$

$$C_{3\_proposed} = 0.75 \le 0.025 f_c' + 0.6\left(1 - \frac{A_s + A_{sr}}{A_g}\right) \le 0.95 \tag{9}$$

The validation of the study's assumptions for high section slenderness CFT column was examined by plotting the results of the compiled test in Tables 1, 2, and 3 in comparison to the AISC column design curve. The distribution of the test results in Fig. 13 indicates the adequacy of the AISC column design equations in estimating the member compressive strength of the CFT columns for a wide range of geometric and material properties.

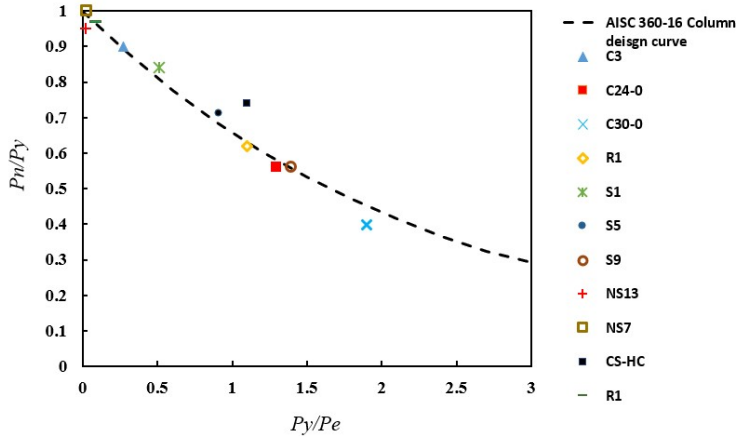

Figure 13: Test results from tables (1), (2), and (3) in comparison with the AISC 360-16 column design curve

4. Conclusions

This paper presented the results of a parametric study that investigated the interaction of section and member slenderness on the behavior and design of high-strength composite filled tube (CFT) members. The parameters of interest included; (1) member slenderness, (2) section slenderness, (3) material strength, (4) section's aspect ratio, and (5) level of axial loading. 2D inelastic fiber analyses were conducted using OpenSees software. Verified effective stress-strain curves were utilized in the section fibers to account for the local buckling of the steel box section and concrete confinement in the high strength CFT members. The following points summarized the results of this paper:

(1) In general, the current AISC code underestimates the section's maximum compressive and flexural strength of high-strength CFT members.
(2) The conservative error using the AISC equations increases as the section slenderness increases.
(3) The study proposed simplified equations and stress blocks for estimating the section's maximum compressive and flexural strength accurately over a wide range of section slenderness ($2 \leq \lambda \leq 5$).
(4) The proposed equations eliminate the need for the current section classification by proposing a continuous function for estimating the compression stress limit of the steel box section due to local buckling.
(5) The paper demonstrates that the strength-slenderness relationship of high-strength CFT columns follows the AISC column design curve in the case of a compact section.
(6) For high-section slenderness, the paper includes a proposal for a more accurate calculation of the concrete contribution in the section's effective stiffness.

5. Future work

The (P-M) interaction curve requires investigation of the curve's peak point mechanism (balance point in the axial-flexure interaction curve). The interaction of the section and member slenderness perhaps requires new equations for the interaction curve. The latter is not even included in the current AISC equations; however, experimental studies demonstrate a reduction of the member strength as the member slenderness increases, which will be evaluated using parametric studies in the future.

6. References

AISC. (2016). "Specification for structural steel buildings." AISC 360-16, Chicago

Lai, Z., Varma, A. H. and Griffis, L. G. (2016) 'Analysis and Design of Noncompact and Slender CFT Beam-Columns', *Journal of Structural Engineering (United States)*, 142(1).

Lai, Z., and Varma, A. H. (2016) 'Effective stress-strain relationships for analysis of noncompact and slender filled composite (CFT) members', *Engineering Structures*. Elsevier Ltd, 124, pp. 457–472.

Lai, Z., and Varma, A. H. (2018) 'High-Strength Rectangular CFT Members: Database, Modeling, and Design of Short Columns', *Journal of Structural Engineering (United States)*, 144(5), pp. 1–18.

Mursi, M. and Uy, B. (2004) 'Strength of slender concrete filled high strength steel box columns', *Journal of Constructional Steel Research*, 60(12), pp. 1825–1848.

Lue, D. M., Liu, J. L. and Yen, T. (2007) 'Experimental study on rectangular CFT columns with high-strength concrete', *Journal of Constructional Steel Research*, 63(1), pp. 37–44.

Patel, V. I., Liang, Q. Q. and Hadi, M. N. S. (2012) 'High strength thin-walled rectangular concrete-filled steel tubular slender beam-columns, Part II: Behavior', *Journal of Constructional Steel Research*, 70, pp. 368–376.

McKenna, F., Fenves, G. L., and Scott, M. H. (2000). “Open system for earthquake engineering simulation.” Univ. of California, Berkeley, CA, ⟨http://opensees.berkeley.edu⟩.

Tao, Z., Wang, Z. Bin and Yu, Q. (2013) ‘Finite element modeling of concrete-filled steel stub columns under axial compression’, *Journal of Constructional Steel Research*, 89, pp. 121–131.

Uy, B. (1998) ‘Local and post-local buckling of concrete filled steel welded box columns’, *Journal of Constructional Steel Research*, 47(1–2), pp. 47–72.

Varma, A. H. *et al.* (2002) ‘Experimental behavior of high strength square concrete-filled steel tube beam-columns’, *Journal of Structural Engineering*, 128(3), pp. 309–318.

Matsui C, Tsuda K, Ishibashi Y. (1995) ‘Slender concrete-filled steel tubular columns under combined compression and bending’. *Proceedings of the 4th Pacific Structural Steel Conference*, Pergamon, Singapore, 3(10), pp.29-36.

Shakir-Khalil H, Zeghiche J. (1989) ‘ Experimental behavior of concrete-filled rolled rectangular hollow-section columns’, *The Structural Engineer,* 67(3), pp. 346-53.

Bridge RQ. (1976) ‘Concrete filled steel tubular columns’. School of Civil Engineering, The University of Sydney, Sydney, Australia, 1976, Research Report No. R 2

Chung J, Tsuda K, Matsui C. High-strength concrete filled square tube columns subjected to axial loading. The Seventh East Asia-Pacific Conference on Structural Engineering & Construction, Kochi, Japan, Vol. 2; 1999. p. 955–60

Liu, D. (2005) ‘Tests on high-strength rectangular concrete-filled steel hollow section stub columns’, *Journal of Constructional Steel Research*, 61(7), pp. 902–911.

Liu, D., Gho, W.-M. and Yuan, J. (2003) ‘Ultimate capacity of high-strength rectangular concrete-filled steel hollow section stub columns’, *Journal of Constructional Steel Research*, 59(12), pp. 1499–1515.

Lai, Z., Varma, A. H. and Zhang, K. (2014) ‘Noncompact and slender rectangular CFT members: Experimental database, analysis, and design’, *Journal of Constructional Steel Research*, 101, pp. 455–468.

Denavit, M. D. *et al.* (2016) ‘Stability Analysis and Design of Composite Structures’, *Journal of Structural Engineering (United States)*. American Society of Civil Engineers (ASCE), 142(3).

Denavit, M. D. *et al.* (2018) ‘Elastic flexural rigidity of steel-concrete composite columns’, *Engineering Structures*. Elsevier Ltd, 160, pp. 293–303.

Denavit, M. D. and Hajjar, J. F. (2014) ‘Characterization of Behavior of Steel-Concrete Composite Members and Frames with Applications for Design’, (July).

"MATLAB 2018b, The MathWorks, Natick,